Computation of Nonclassical Solutions to Hamilton-Jacobi Problems

PIERRE-ALAIN GREMAUD* AND NICHOLAS R. IDE†

Abstract. This paper is devoted to the construction of numerical methods for the approximation of nonclassical solutions to multidimensional Hamilton-Jacobi equations, for both scalar and vectorial problems. Recent theoretical results have yielded existence of solutions in many cases for which the usual viscosity approach was ill-suited or not applicable. The selection criterion used here is based on a viscoelasticity/capillarity approach, common in Solid Mechanics. Numerical methods adapted to this framework are built. Consistency of the model equation with the given selection criterion is essential. It is achieved here through the use of high order finite difference schemes. By considering applications to potential well problems, the convergence of the methods are investigated.

Key words. Hamilton-Jacobi, viscosity solution, nonconvex, systems, numerical viscosity

AMS(MOS) subject classifications. 65M60, 65N30, 35L65

1. Introduction. This paper presents some numerical experiments related to the computation of solutions to nonlinear Hamilton-Jacobi (HJ) scalar and vectorial equations, in the two-dimensional case. More precisely, we consider the following HJ equation with Dirichlet boundary condition

$$\begin{aligned} F(\nabla u(x)) &= 0 \qquad \text{a.e. in } x \in \Omega, \\ u(x) &= \varphi(x) \qquad x \in \partial\Omega, \end{aligned} \tag{1.1}$$

where Ω is an open bounded set in $\mathbb{R}^2$, $u : \Omega \to \mathbb{R}^m$, $F : \mathbb{R}^{m\times 2} \to \mathbb{R}$, $\varphi \in W^{1,\infty}(\Omega)^m$, and

$$\nabla u(x) = \begin{pmatrix} \dfrac{\partial u_1}{\partial x_1}(x) & \dfrac{\partial u_1}{\partial x_2}(x) \\ \cdots & \cdots \\ \dfrac{\partial u_m}{\partial x_1}(x) & \dfrac{\partial u_m}{\partial x_2}(x) \end{pmatrix}.$$

We refer to (1.1) as being vectorial if $m > 1$, and scalar if $m = 1$, (u is then a scalar). As is well known, (1.1) does not, in general, admit classical solutions, i.e., $u \in \mathcal{C}^1(\Omega)^m$. The above problem (1.1) has been extensively studied, although mostly in the scalar case $m = 1$, see e.g. [6, 7, 21, 20].

The calculations presented here stem from new theoretical results recently obtained by B. Dacorogna and P. Marcellini [8, 9]. Their approach is totally different from the usual viscosity approach. We start by focusing on the role played by this latter criterion.

The notion of viscosity solution, see e.g. [6], has been widely and successfully used. This concept is here consistent with vanishing viscosity solutions, i.e.

$$\begin{aligned} -\varepsilon\Delta u_\varepsilon + F(\nabla u_\varepsilon) &= 0 \qquad \text{in } \Omega, \\ u_\varepsilon &= \varphi \qquad \text{on } \partial\Omega, \end{aligned} \tag{1.2}$$

* Center for Research in Scientific Computation and Department of Mathematics, North Carolina State University, Raleigh, NC 27695-8205. Partially supported by the Army Research Office through grants DAAH04-95-1-0419 and DAAH04-96-1-0097, and by the North Carolina Supercomputing Center.

† Department of Mathematics, North Carolina State University, Raleigh, NC 27695-8205. Present address: Lincoln Lab, MIT, Lexington, MA 02173-9108.

where $\varepsilon > 0$ is the vanishing viscosity.

In the scalar case, and if the Hamiltonian F is convex, the problem is remarkably well understood. Indeed, if F is assumed to be convex, continuous and to satisfy some growth conditions (see e.g. [21, Th. 6.2, p.152, for details and proof]), one has

• (1.2) admits a unique solution u_ε; u_ε converges to a function $u \in W^{1,\infty}(\Omega)$ in $L^p(\Omega)$, $1 \leq p < \infty$, and $L^\infty(\Omega)$ weak $\star$;

• the limit function u satisfies

$$\begin{aligned} F(\nabla u(x)) &= 0 \qquad \text{a.e. in } x \in \Omega, \\ u(x) &= \tilde{\varphi}(x) \qquad x \in \partial\Omega; \end{aligned} \tag{1.3}$$

• if φ can be extended to Ω into a $W^{1,\infty}(\Omega)$ function, still denoted φ, such that

$$F(\nabla \varphi(x)) \leq 0 \qquad \text{a.e. in } x \in \Omega, \tag{1.4}$$

then $\tilde{\varphi} = \varphi$ in (1.3), and thus u solves (1.1).

Note that if (1.4) is not satisfied, one should not expect the boundary condition to be satisfied pointwise, but in a much weaker *viscous* sense (see e.g. [6, def. 7.4], or Section 2). Note also that if the Hamiltonian F is not convex and/or in the vectorial case ($m > 1$), the problem is a lot more difficult.

The results in [8, 9], which are based on the use of Baire's Theorem and the notion of quasiconvexity, are existence results. It is shown, under very general assumptions (see Section 2 for some examples) that Lipschitz solutions, $u \in W^{1,\infty}(\Omega)^m$ to (1.1), satisfying the boundary condition (1.1.2) in the *classical* sense, may exist even if (1.4) is *not* satisfied. Those results apply to the vectorial case as well, for which the notion of viscosity condition is not very well suited, because it uses ordering of values taken by u (maximal solution, for instance).

We are interested here in problems for which the well known boundary layer type of behavior of the viscosity solutions is to be avoided (on physical grounds, for instance; see examples below). For such problems, other selection mechanisms have to be introduced. For given applications, candidates will be selected among the usual infinity of existing solutions through energy considerations for instance. Two criteria, relatively standard for material science problems, are viscoelastic damping [28, 33] and capillarity [22, 19, 29]. Accordingly, the solutions sought here are viscoelasticity/capillarity solutions. We strongly emphasize that this paper aims at designing efficient numerical methods once a selection criterion has been chosen. Along the way, unifying principles governing the approximation process are sought. The relative merits of various selection criteria are *not* discussed. We note however that the approach taken has very strong connexions with dynamical models of martensitic phase transitions in solids [22, 29]. For other recent examples of non classical solutions, see for instance, in the case of conservation laws, [14] and the references quoted therein.

The outline of the paper is follows. In Section 2, the definition of viscosity solution is recalled, and three examples are introduced and analyzed. Viscoelastic damping and capillarity are introduced and discussed in Section 3. Section 4 is devoted to the design and study of a numerical method. We present the computational results in Section 5. Final remarks are offered in Section 6.

2. Examples. In this section, the formal definition of viscosity solution is recalled, and three main examples are presented.

In the scalar case, i.e. $m = 1$, a function u is called a viscosity solution to (1.1) if it is continuous, and if [6, def. 7.4]

$$
\begin{aligned}
F(p) &\le 0 &\quad& \forall p \in D^+u(x), x \in \Omega, && (2.1.1)\\
F(p) \wedge (u(x) - \varphi(x)) &\le 0 && \forall p \in D^+u(x), x \in \partial\Omega, && (2.1.2)\\
F(p) &\ge 0 && \forall p \in D^-u(x), x \in \Omega, && (2.1.3)\\
F(p) \vee (u(x) - \varphi(x)) &\ge 0 && \forall p \in D^-u(x), x \in \partial\Omega, && (2.1.4)
\end{aligned}
$$

where $a \wedge b = \min\{a, b\}$, $a \vee b = \max\{a, b\}$, and where $D^{\pm}u$ are the super and subdifferentials

$$
D^{\pm}u(x_0) = \{a \in \mathbb{R}^2; \lim_{x \to x_0} \frac{(u(x) - u(x_0) - a \cdot (x - x_0))^{\pm}}{|\, x - x_0 \,|} = 0\}.
$$

Note that (2.1.2) and(2.1.4) correspond to satisfying the boundary condition in the "viscous sense", a rather weak sense (see Example 2, below).

Example 1: a scalar convex example. We consider first the Eikonal equation [20, 21]

$$
\begin{aligned}
\|\nabla u\| &= 1 \qquad \text{a.e. in } \Omega,\\
u &= 0 \qquad \text{on } \partial\Omega.
\end{aligned}
\tag{2.2}
$$

As is well known, and as a direct consequence of the classical Huygens' principle, the unique viscosity solution is here

$$
u(x) = \mathrm{dist}(x, \partial\Omega),
\tag{2.3}
$$

see Figure 2.1. The problem can be rewritten in the form (1.1) by setting $\varphi = 0$ and with Hamiltonian $F : \mathbb{R}^2 \to \mathbb{R}$ given by

$$
F(\xi_1, \xi_2) = (\xi_1^2 + \xi_2^2 - 1)^2,
\tag{2.4}
$$

In particular, all the standard assumptions related to the scalar convex case mentioned in Section 1. are satisfied.

Example 2: a scalar nonconvex example. For a general scalar problem of the type (1.1), the results in [8, 9] yield the existence of a solution $u \in W^{1,\infty}(\Omega)$ provided that $\varphi \in \mathcal{C}^1(\Omega)$ and that for any $x \in \Omega$

$$
\nabla\varphi(x) \in \mathrm{int\,co}\{\xi \in \mathbb{R}^2; F(\xi) = 0\} \cup \{\xi \in \mathbb{R}^2; F(\xi) = 0\},
\tag{2.5}
$$

where int co denotes the interior of the convex hull of a given set. No assumption is made on F, be it convexity, coercivity or continuity. Note also that (2.5) is more general than (1.4).

As a specific example, we consider the problem of finding $u \in W^{1,\infty}(\Omega)$ such that

$$
\begin{aligned}
|\frac{\partial u}{\partial x_1}| = |\frac{\partial u}{\partial x_2}| &= 1 \qquad \text{a.e. in } \Omega,\\
u &= 0 \qquad \text{on } \partial\Omega.
\end{aligned}
\tag{2.6}
$$

This can be rewritten as (1.1), with $\varphi = 0$ and with Hamiltonian $F : \mathbb{R}^2 \to \mathbb{R}$ given by

$$
F(\xi_1, \xi_2) = |\,|\xi_1| - 1\,| + |\,|\xi_2| - 1\,|,
\tag{2.7.1}
$$

or

$$F(\xi_1, \xi_2) = (\xi_1^2 - 1)^2 + (\xi_2^2 - 1)^2. \tag{2.7.2}$$

The function F is nonconvex and the compatibility condition (1.4) is not satisfied. If $\Omega = (0,1)^2$, one can readily check that

$$u(x,y) = -1 + |\, x - 1/2 \,| + |\, y - 1/2 \,|, \tag{2.8}$$

is a viscosity solution, i.e., it satisfies (2.1). The boundary condition is however only satisfied at the four corners, see Figure 2.1. This is nevertheless consistent with "satisfying the boundary conditions in a viscous sense", see (2.1.2, 2.1.4).

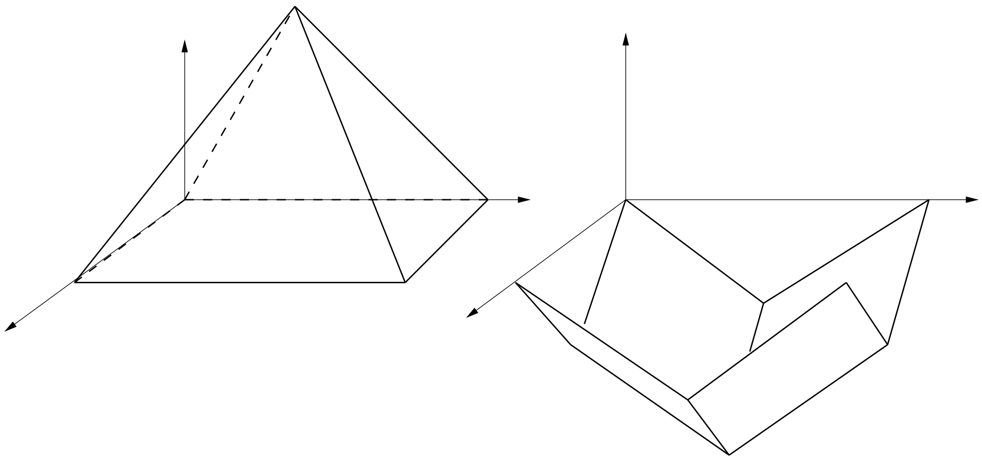

FIGURE 2.1. *Viscosity solutions for Example 1 (left) and Example 2 (right) when* $\Omega = (0,1)^2$.

The condition (2.5) is however verified, and thus there exists functions $u \in W_0^{1,\infty}(\Omega)$, solutions of (2.6), where the boundary condition is satisfied in the classical sense. Such a solution is computed in Section 5 (see also Figure 5.7).

It is interesting to consider the same problem as above, but in a rotated domain $\tilde{\Omega}$, where $\tilde{\Omega}$ has its sides parallel to the main diagonals $y = x$ and $y = -x$; for instance $\tilde{\Omega} =$ square with vertices $\{(0,0), (1/\sqrt{2}, 1/\sqrt{2}), (0, \sqrt{2}), (-1/\sqrt{2}, 1/\sqrt{2})\}$. Here

$$u(x,y) = -\frac{1}{\sqrt{2}} + |\, x \,| + |\, y - \frac{1}{\sqrt{2}} \,|,$$

is a viscosity solution. The boundary condition is classically satisfied everywhere.

Example 3: a vectorial nonconvex example. We consider the so-called prescribed singular values problem. This corresponds to a vectorial example of (1.1) ($m = 2$). A function $u \in W^{1,\infty}(\Omega)^2$ is sought such that

$$\mu_i(\nabla u) = a_i \qquad \text{a.e. in } \Omega, i = 1, 2, \tag{2.9.1}$$

$$u = \varphi \qquad \text{on } \partial\Omega, \tag{2.9.2}$$

where $0 \le \mu_1(\nabla u) \le \mu_2(\nabla u)$ denote the singular values of ∇u, i.e., the eigenvalues of the matrix $(\nabla u^T \nabla u)^{1/2}$.

By definition of the singular values, (2.9.1) is equivalent to

$$\|\nabla u\|^2 = a_1^2 + a_2^2 \qquad \text{a.e. in } \Omega, \tag{2.10.1}$$
$$|\det \nabla u| = a_1 a_2 \qquad \text{a.e. in } \Omega, \tag{2.10.2}$$

where $\|\cdot\|$ stands for the Frobenius norm.

Note that this can be rewritten as a HJ problem of the general type (1.1) where $F : \mathbb{R}^{2\times 2} \to \mathbb{R}$ and $F = F_1^2 + F_2^2$ with

$$F_1(\nabla u) = \|\nabla u\|^2 - a_1^2 - a_2^2, \qquad F_2(\nabla u) = |\det \nabla u| - a_1 a_2. \tag{2.11}$$

Finally, (2.9) is also related to a potential well problem. If for instance $a_1 = a_2 = 1$, then (2.9.1) becomes

$$\nabla u(x) \in SO_2\,\mathbb{I} \cup SO_2\,\mathbb{I}_- \qquad \text{a.e. in } \Omega, \tag{2.12}$$

where $\mathbb{I} = \begin{pmatrix} 1 & 0 \\ 0 & 1 \end{pmatrix}$ and $\mathbb{I}_- = \begin{pmatrix} 1 & 0 \\ 0 & -1 \end{pmatrix}$, and where SO_2 is the set of orthogonal matrices with determinant equal to 1. Again, the results in [8, 9] yield the existence of Lipschitz solutions to (2.6) under mild conditions on φ (in the simplified case $a_1 = a_2 = 1$: $\varphi \in W^{1,\infty}(\Omega)^2$ such that for some $\delta > 0$, $\mu_2(\nabla\varphi) \leq 1 - \delta$, a.e.

Potential well problems have recently received a lot of attention, mainly because of their strong connexion with material microstructures. In that respect, it should be noticed that just prescribing the singular values of the deformation gradient ∇u is not physically satisfactory. Indeed, orientation reversing transformations are not excluded since a matrix ∇u with singular values a_1 and a_2 can be either proper, i.e., $\det \nabla u = a_1 a_2$ or improper, i.e., $\det \nabla u = -a_1 a_2$. The reader is referred to [2, 4, 22] and the references quoted therein, for respectively, material sciences, mathematical and computational approaches. See also [25] for a scalar application.

3. Viscoelastic damping and capillarity.

We consider a selection criterion based on the use of regularized dynamical problems.

The first step consists in realizing that (1.1) can be rewritten as

$$\inf_{u \in W_0^{1,\infty}(\Omega)^d + \varphi} \mathcal{E}(u), \tag{3.1}$$

where $\mathcal{E}(u) = \int_\Omega F(\nabla u)\,dx$. The central conjecture is as follows. We would like to construct a dynamical system $T(t)$ of some sort admitting $\mathcal{E}$ as Lyapunov function. More precisely, for any initial condition u_0 and $\{t_j\}$, $t_j \to \infty$, $T(t_j)\,u_0$ should be a minimizing sequence for $\mathcal{E}$, see [1] for very general remarks about the above approach.

A natural family of problems can be formally derived by adding to the "elastic" energy, a kinetic energy, leading to

$$E(u) = \frac{1}{2}\int_\Omega |\partial_t u|^2\,dx + \int_\Omega F(\nabla u)\,dx, \tag{3.2}$$

and the corresponding equation of motion

$$\partial_{tt} u - \operatorname{div}\, \sigma(\nabla u) = 0 \qquad \text{in } \Omega \times \mathbb{R}^+, \tag{3.3}$$

where $\sigma = DF$, or equivalently

$$\begin{aligned} &\partial_t v - \operatorname{div}\, \sigma(\nabla u) = 0, \\ &\partial_t u = v. \end{aligned} \tag{3.4}$$

In the case of our three examples, we have respectively

$$(\xi_1,\xi_2) = 4(\xi_1^2+\xi_2^2-1)\begin{pmatrix}\xi_1\\ \xi_2\end{pmatrix}, \tag{3.5}$$

$$\sigma(\xi_1,\xi_2) = \begin{pmatrix}4\xi_1(\xi_1^2-1)\\ 4\xi_2(\xi_2^2-1)\end{pmatrix}, \tag{3.6}$$

$$\sigma(A) = 4F_1(A)\,A + 2F_2(A)\,\tilde{A}, \tag{3.7}$$

where for example (2.6) the Hamiltonian given is by (2.7.2)), F_1 and F_2 are defined in (2.11), and

$$A = \begin{pmatrix}\xi_{11} & \xi_{12}\\ \xi_{21} & \xi_{22}\end{pmatrix}, \qquad \tilde{A} = \operatorname{sign}(\det A)\begin{pmatrix}\xi_{22} & -\xi_{21}\\ -\xi_{12} & \xi_{11}\end{pmatrix}.$$

By multiplying (3.4.1) by v and integrating over Ω, it is easily checked that (3.4) (and/or (3.3)) leaves E invariant, i.e., $\dfrac{dE}{dt}(u) = 0$, for any $t > 0$ (since the boundary condition φ is time independent).

As a first step toward a selection criterion, we consider the *regularized* equation of motion, namely

$$\partial_{tt}u - \operatorname{div}\,\sigma(\nabla u) = \mu\Delta\partial_t u \qquad \text{in } \Omega\times\mathbb{R}^+. \tag{3.8}$$

In that case, a similar calculation as above yields

$$\frac{dE}{dt}(u) = -\mu\int_\Omega |\,\nabla v\,|^2\,dx. \tag{3.9}$$

It is known that for fairly general functions σ and constant $\mu > 0$, the above problem (3.8) admits a unique strong solution (in particular, the conditions on σ do not involve any convexity argument, see [10, 28]). After rescaling of the time, we may set $\mu = 1$. Unlike what was done in [33], we do not attach any physical meaning to (3.8), and the corresponding dynamics. We are merely interested in using it as a tool to select a stationary solution to (1.1) (see also [18]).

Many conjectures and assumptions have been made about the relationship between the solutions to (3.8) or (3.10), below, and (1.1). It is possible to show that the dynamics corresponding to (3.8) prevent the propagation, creation or annihilation of singularities of the gradient of the solution [29]. Those results were inspired by the numerical experiments in [33], with which they seem, at least partially, to agree. Accordingly, a capillarity term is often considered, leading to the equation ($\mu = 1$)

$$\partial_{tt}u - \operatorname{div}\,\sigma(\nabla u) = \Delta\partial_t u - \delta^2\Delta^2 u \qquad \text{in } \Omega\times\mathbb{R}^+. \tag{3.10}$$

The energy has to be modified to

$$E(u) = \frac{1}{2}\int_\Omega |\,\partial_t u\,|^2\,dx + \int_\Omega F(\nabla u)\,dx + \frac{\delta^2}{2}\int_\Omega |\,\Delta u\,|^2\,dx, \tag{3.11}$$

and again, it varies according to (3.9).

We know of no asymptotic results for (3.10) in the above multidimensional case, [30]. In the quasistatic case, i.e., with inertia neglected (no term $\partial_{tt}u$ in (3.10)), convergence to equilibria of the functional energy as t goes to infinity has been established, provided that the total initial energy is low, the wells of F not too deep, and the capillarity coefficient $\delta > 0$ not too small, see [31] for details. Partial one-dimensional results can also be found in [11].

4. Discretization. The methods to be described below are used on uniform Cartesian grids. Owing to the complex character of the solutions sought, no efforts have been made to adapt the spatial grid, in order to avoid unwelcome interferences due to the adaption process itself (namely, spurious oscillations).

A generic spatial cell will be $[x_j, x_{j+1}] \times [y_k, y_{k+1}]$, where $x_{j+1} - x_j = y_{k+1} - y_k = \Delta x$. The time step is denoted Δt.

The choice of a numerical method is guided by the two following criteria

(1) *the scheme must admit (3.10) as model equation,*

(2) *as $t \to \infty$, one should reach a solution of (1.1), i.e., "the asymptotics should be right".*

Obtaining a scheme admitting the correct model equation is easily achieved by approximating all the terms in (3.10) to a high enough order. More precisely, we choose our discretization so that no derivatives of u of order less than four appear in the model equation. Roughly speaking, this means that no additional diffusion or capillarity/surface tension effects are implicitly added through the discretization process. Note, however, that all this is formal. Indeed, the underlying idea is that the lower order terms are the dominant ones in the model equation, which makes sense only in the presence of smooth solutions.

Accordingly, we use a third order approximation of the time derivative, a third order approximation of the first derivative in space, a fourth order approximation of the second order space derivatives, and a second order approximation of the fourth order space derivatives. More precisely

$$\partial_t u(\cdot, t_n) \approx \left(\frac{11}{6} u(\cdot, t_n) - 3u(\cdot, t_{n-1}) + \frac{3}{2} u(\cdot, t_{n-2}) - \frac{1}{3} u(\cdot, t_{n-3})\right) \frac{1}{\Delta t}, \tag{4.1}$$

$$\partial_x u(x_j, \cdot) \approx \Big(u(x_{j-2}, \cdot) - 8u(x_{j-1}, \cdot) + 8u(x_{j+1}, \cdot) - u(x_{j+2}, \cdot)\Big) \frac{1}{12\Delta x}, \tag{4.2}$$

$$\partial_{xx} u(x_j, \cdot) \approx \Big(-u(x_{j-2}, \cdot) + 16u(x_{j-1}, \cdot) - 30u(x_j, \cdot) + 16u(x_{j+1}, \cdot) - u(x_{j+2}, \cdot)\Big) \frac{1}{12\Delta x^2}, \tag{4.3}$$

$$\partial_{xxxx} u(x_j, \cdot) \approx \Big(u(x_{j-2}, \cdot) - 4u(x_{j-1}, \cdot) + 6u(x_j, \cdot) - 4u(x_{j+1}, \cdot) + u(x_{j+2}, \cdot)\Big) \frac{1}{\Delta x^4}, \tag{4.4}$$

The reader will have recognized (4.1) as the 3-rd order BDF method, see e.g. [12], p.311. As is well known, the method is nearly A-stable [13, Chap. 5], [32, p.494] and thus has nice stability properties, regardless of the size of the time step Δt. It is well suited for integrating stiff problems. The nonlinear problems to be solved at each time step are handled by Inexact-Newton-Armijo iterations, with restarted GMRES as linear solver [17, p.138–144]. Both absolute and relative error tolerances for the nonlinear solver were set equal to Δx^2. The use of (4.2) and the corresponding formula in y for the discretization of the nonlinear term div $\sigma(\nabla u)$ in (3.4) leads to a rather large stencil in the two dimensional case. At and/or near the boundary, the above stencils are modified, so that no more than one order is lost due to the boundary conditions. The reader is referred to [3, 5] for other examples of numerical methods based on specific model equations.

Let us now turn to our second criterion (necessity to have the "right asymptotics"). This point is rather delicate. Indeed, the discretized system has in general many more parameters than the original one (time step, etc...). This process is not fully transparent, and might result in discretized systems exhibiting very complicated dynamical properties. Typically, distortion, shrinkage and segmentation of the basin of attraction of the true steady solution(s) can be observed. Convergence to spurious steady solutions, spurious limit cycles, slow convergence, or nonconvergence can result. Even when theoretical results exist, those tend to deal with the case $\Delta t \to 0$ and number of steps $n \to \infty$, rather than with Δt "fixed", and $n \to \infty$, as in the case in practice. Multistep methods, as the one used here, seem to present some advantages over popular Runge-Kutta methods: the former have the same fixed points as the original equation, while the later may exhibit additional spurious fixed points [16]. The situation is not fully understood; see however [34, 35] for some interesting computational experiments.

In order to get a rough idea of the stability properties of our scheme, we perform an analysis of the semidiscrete scheme, on the one hand, as well as a linear stability study on the other hand. For the sake of simplicity, and since the quality of the information obtained this way is limited, both studies are done in a infinite one-dimensional domain.

In case $\Omega = \mathbb{R}$, the semidiscrete scheme takes the form

$$\frac{d}{dt}v_j = \frac{1}{\Delta x}M_1\sigma(\frac{1}{\Delta x}M_1u_j) + \frac{1}{\Delta x^2}M_2v_j - \frac{\delta^2}{\Delta x^4}M_4u_j, \tag{4.5}$$

$$\frac{d}{dt}u_j = v_j, \tag{4.6}$$

where

$$\begin{aligned} M_1 &= \frac{1}{12}(S_{-2} - 8S_{-1} + 8S_1 - S_2), \\ M_2 &= \frac{1}{12}(-S_{-2} + 16S_{-1} - 30S_0 + 16S_1 - S_2), \\ M_4 &= (S_{-2} - 4S_{-1} + 6S_0 - 4S_1 - S_2), \end{aligned}$$

where S_j is the shift operator, i.e, $S_ju_i = u_{i+j}$. The following relations hold

$$\begin{aligned} M_2 &= S_{-1} - 2S_0 + S_1 - \frac{1}{12}(S_{-1} - 2S_0 + S_1)^2 = \tilde{M}_2 - \frac{1}{12}\tilde{M}_2^2, \\ M_4 &= \tilde{M}_2^2, \\ \tilde{M}_2 &= S_{-1} - 2S_0 + S_1 = (-S_{-1} + S_0)(-S_0 + S_1), \end{aligned}$$

where $\tilde{M}_2$ is the operator entering in the classical second order three-point formula for ∂_{xx}. Proceeding now as in the previous section, we multiply (4.5) by $v_j\Delta x$ and sum over j. Some elementary algebraic manipulations lead to

$$\frac{dE_h}{dt} = -\sum_{j\in\mathbb{Z}}\left(\frac{S_1 - S_0}{\Delta x}v_j\right)^2\Delta x - \frac{\Delta x^2}{12}\sum_{j\in\mathbb{Z}}\left(\frac{1}{\Delta x^2}\tilde{M}_2v_j\right)^2\Delta x, \tag{4.7}$$

where the discrete energy E_h is defined as

$$E_h = \frac{1}{2}\sum_{j\in\mathbb{Z}}(v_j)^2\,\Delta x + \sum_{j\in\mathbb{Z}} F(\frac{1}{\Delta x}M_1 u_j)\,\Delta x + \frac{\delta^2}{2}\sum_{j\in\mathbb{Z}}\left(\frac{1}{\Delta x^2}\tilde{M}_2 u_j\right)^2 \Delta x. \tag{4.8}$$

The relations (4.8) and (4.7) are clearly the discrete counterparts of (3.11) and (3.9), respectively.

We now perform a linear stability study, i.e., the stress $\sigma(\xi)$ is linearized to $\sigma_i'\xi$. In order to find the amplification matrix, we consider a single harmonic $u^n\, e^{ij\phi}$, where j denotes a node of the spatial grid. As noticed by several authors, the von Neumann type stability analysis considered here, although "incomplete", usually leads to relevant information, even when the boundary conditions are ignored [15, Chap. 10], [23]. After introduction of the auxiliary variables

$$v^n = u^{n-1},\, w^n = u^{n-2},\, x^n = u^{n-3},\, y^n = u^{n-4},\, z^n = u^{n-5},$$

the fully discrete one-dimensional scheme can be rewritten $U^{n+1} = GU^n$, where $U = [u\,v\,w\,x\,y\,z]^T$ and

$$G = \begin{pmatrix} b_0 & b_1 & b_2 & b_3 & b_4 & b_5 \\ 1 & 0 & 0 & 0 & 0 & 0 \\ 0 & 1 & 0 & 0 & 0 & 0 \\ 0 & 0 & 1 & 0 & 0 & 0 \\ 0 & 0 & 0 & 1 & 0 & 0 \\ 0 & 0 & 0 & 0 & 1 & 0 \end{pmatrix}$$

with

$$\begin{aligned} b_0 &= \left(6 + \frac{18r}{11}(15 - 16\cos\phi + 2\cos 2\phi)/6\right)/b, \\ b_1 &= \left(-\frac{87}{11} - \frac{9r}{11}(15 - 16\cos\phi + 2\cos 2\phi)/6\right)/b, \\ b_2 &= \left(\frac{184}{33} + \frac{2r}{11}(15 - 16\cos\phi + 2\cos 2\phi)/6\right)/b, \\ b_3 &= \frac{-51}{22\,b}, \\ b_4 &= \frac{6}{11\,b}, \\ b_5 &= \frac{-2}{33\,b}, \end{aligned}$$

where

$$\begin{aligned} b = \frac{11}{6} &+ r(15 - 16\cos\phi + 2\cos 2\phi)/6 \\ &+ \frac{sr}{132}(65 - 16\cos\phi - 64\cos 2\phi + 16\cos 3\phi - \cos 4\phi), \\ &+ d(6 - 8\cos\phi + 2\cos 2\phi), \end{aligned}$$

and where we have set $r = \dfrac{\Delta t}{\Delta x^2}$, $s = \Delta t\sigma'$, $\mu = 1$, $d = \delta^2\dfrac{\Delta t}{\Delta x^4}$; ϕ is the phase angle.

It is then possible to investigate, numerically, for which values of the parameters r, s and δ the matrix G has its spectral radius $\rho(G)$ less than one, for all phase angle ϕ. In Figure 4.1, the spectrum of G is represented in the complex plane. It is observed numerically that the parameter r only affects the distribution of the eigenvalues inside the unit circle, but not whether those are inside or outside of the circle. This is a direct consequence of the implicitness of the scheme. The parameter s, on the other hand, affects the linear stability. For s "small", the scheme is stable, for s "large", it is not. Values of $s \lessapprox 10$, appear to be stable. Finally, for "small values" of d, i.e., $\lessapprox 1$, the parameter δ has a regularizing effect. As shown in Figure 4.1, most of the eigenvalues with real part close to close to 1, when $\delta = 0$, are eliminated for $\delta > 0$. In agreement with the above remarks, the calculations presented in this paper were performed under a stability condition of the type $\Delta t \, \|\sigma'\|_\infty = \mathcal{O}(1)$, where $\|\sigma'\|_\infty = \max_i \| \sigma'(\nabla u_h) \|_\infty$, u_h being the numerical solution.

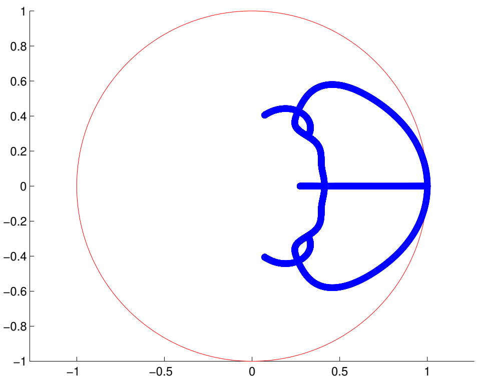

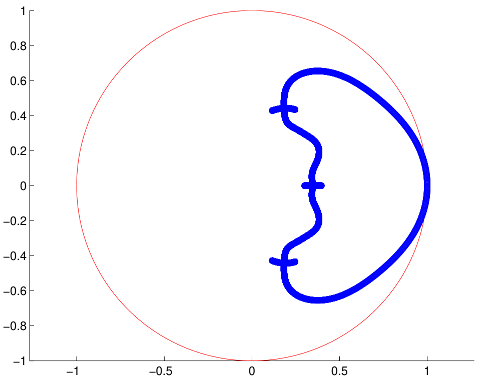

FIGURE 4.1. *Distribution of the eigenvalues of the amplification matrix for 1000 uniformly distributed phase angles in $[-\pi, \pi]$, for $r = s = 1$, $d = 0$ (left) and $d = .2$ (right).*

In the calculations below, the added stability due to the capillarity term $\delta \Delta^2 u$ was of importance. Without that term, (small) oscillations of various kinds would prevent a clean convergence. Therefore, our algorithm consists in solving (3.10) using the method described above, for small values of δ. The stopping criterion in time used throughout was that the kinetic energy be small enough, namely

$$\frac{1}{2} \int_\Omega v_h^2 \, dx < 10^{-6},$$

where v_h stands for the discrete velocity. When the complexity of the problem allowed, smaller values were used.

The feasibility of the method is shown on the one-dimensional example corresponding to both(!) our Examples 1 and 2, in case $\Omega = (-1, 1)$, see Figure 4.2, below. Numerically, it appears that the (L^1-norm of the) residual, obtained by plugging the converged solution into (1.1), is of order $\mathcal{O}(\delta)$. Although conjectures have been made [19, 25] (see also next section), there are, to the authors' knowledge, no complete result related to the convergence when the capillarity coefficient δ tends to zero.

In the next section, the initial conditions for u are generated by solving once the viscous problem (1.2) for a "large" ε, $\varepsilon = 1$. The initial velocity is chosen as uniformly zero.

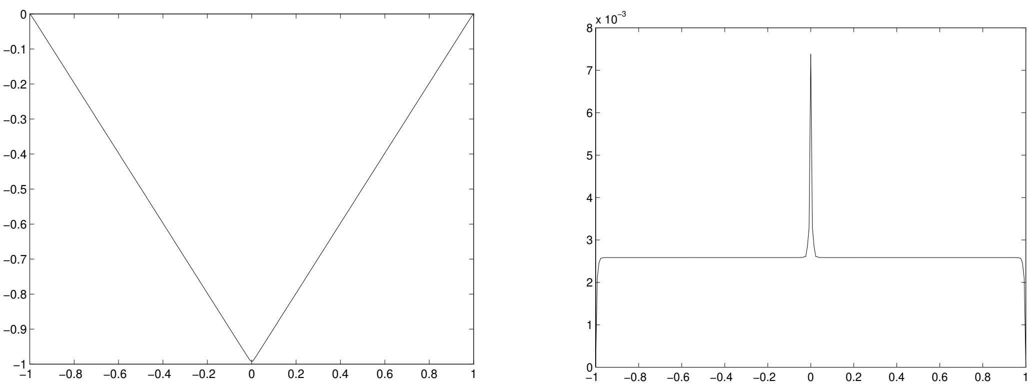

FIGURE 4.2. *Converged solution (left) for $\Delta x = 2/256$ and $\delta = 0.01$, together with the difference between the numerical solution and the exact solution $u(x) = |x| - 1$ (right). The initial condition was chosen as $x^2 - 1$.*

5. Numerical results. Numerical results corresponding to the examples of §2 are presented in this section. The calculations were performed on a Sun SPARC 20 workstation.

We start with two preliminary remarks. First, most "reasonable" numerical methods when applied to the obvious time dependent problem

$$\partial_t u + F(\nabla u) = 0 \qquad \text{in } \Omega \times \mathbb{R}^+, \tag{5.1}$$

appear to converge, for scalar problems and large times, to the viscosity solution. More precisely, ENO schemes [26, 27] can be used to generate approximations to the respective viscosity solutions of the two scalar examples of §2. The converged solution corresponding to Example 2, and obtained by a second order TVD scheme is displayed in Figure 5.1.

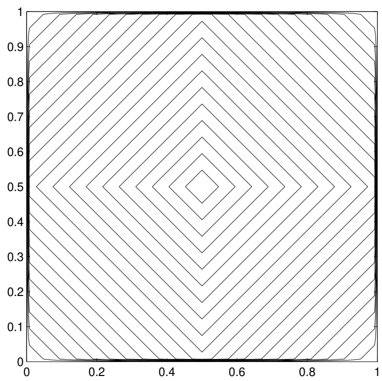

FIGURE 5.1. *Converged solution for Example 2 obtained by a second order TVD scheme applied to (5.1).*

Note that although the above convergence remark might seem obvious, it has, to the authors' knowledge, still not been established theoretically.

Second, in what follows, what is referred to as *residual* is an approximation to

$$\int_\Omega F(\nabla u_h)\, dx.$$

The calculation of the above quantity does not play any role in the algorithm itself, but is merely an a posteriori quality control. If, on a cell K, the values at the four corners are, counterclockwise, u_1, u_2, u_3 and u_4, two approximations for each of $\partial_x u$ and $\partial_y u$ are easily obtained: $\partial_x u \approx (u_2 - u_1)/\Delta x = D_x^- u_h$, $\partial_x u \approx (u_3 - u_4)/\Delta x = D_x^+ u_h$, ... Then we set

$$F(\nabla u_h)|_K \approx \Big(F(D_x^- u_h, D_y^- u_h) + F(D_x^- u_h, D_y^+ u_h) + F(D_x^+ u_h, D_y^- u_h) + F(D_x^+ u_h, D_y^+ u_h) \Big)/4.$$

In the above formula, the above order of the evaluation and averaging operations should of course not be reversed, see [24] on related questions.

Example 1: a scalar convex example.

As noticed earlier, the viscosity solution is here $u(x) = \operatorname{dist}(x, \partial\Omega)$. Figure 5.2 illustrates the convergence of the numerical solution toward a steady state solution precisely corresponding to u, this for $\Omega = (0,1)^2$.

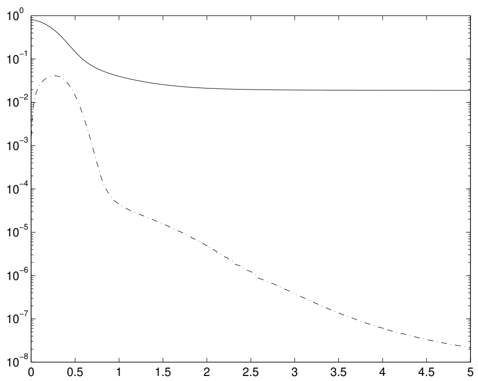

FIGURE 5.2. *Example 1. Decay of the residual (solid line) and kinetic energy; $\Omega = (0,1)^2$, $\Delta x = 1/128$, $\Delta t = .001$, and $\delta = .01$.*

A quick calculation shows that if $\Omega = (0,1)^2$ is partitioned using a uniform Cartesian grid of size Δx, then the optimal (L^1-norm of the) residual is approximately equal to $2\Delta x$. On the grid used in Figure 5.2, this corresponds to an optimal value of $1/64 = .015625$. The actual residual at time $t = 5$ is about .01896. Note that on this simple example, our results would obviously have greatly benefited from an adaption of the mesh. However, the adaption process itself might interfere, when seeking whether (and how) fine structures appear in the problems below.

Contour plots of the numerical solution u and the corresponding velocity v are displayed in Figure 5.3. In that picture, the order of magnitude of the velocity is about $|\,v\,|_\infty \approx 6 \times 10^{-4}$.

In the present case of the Eikonal equation, it is very tempting to assume that when convergence to a solution of (1.1) occurs as $t \to \infty$, the limit solution would be the viscosity solution. This is indeed what we observe in Figure 5.3, where the numerical solution approaches $u(x) = \operatorname{dist}(x, \partial\Omega)$, the viscosity solution of (2.2). For similar problems, but with the dynamical selection criterion being replaced by a surface energy term, i.e.

$$\min \int_{\Omega} (F(\nabla u) + \epsilon^2 |\nabla\nabla u|^2)\, dx, \tag{5.2}$$

it was conjectured in [25] that $u_\epsilon \to \operatorname{dist}(x, \partial\Omega)$ as $\epsilon \to 0$, where u_ϵ is a solution to (5.2). In [19], it was suggested that the conjecture is probably true if Ω is convex, and probably incorrect in case Ω is not convex. This question will be addressed elsewhere.

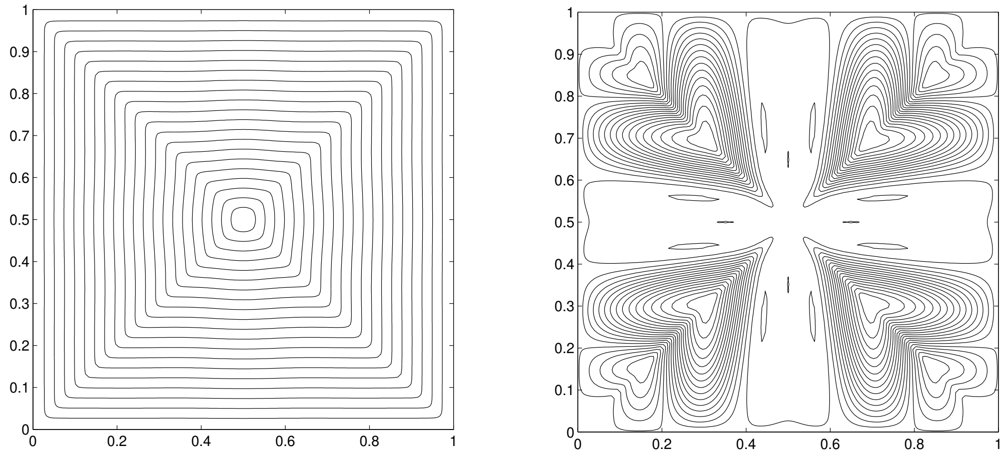

FIGURE 5.3. *Example 1. Computed solution u (left), and corresponding velocity v;* $\Omega = (0,1)^2$, $\Delta x = 1/128$, $\Delta t = .001$, *and* $\delta = .01$.

Example 2: a scalar nonconvex example. The same numerical parameters as above were used. The behavior of the residual and the kinetic energy are shown in Figure 5.4.

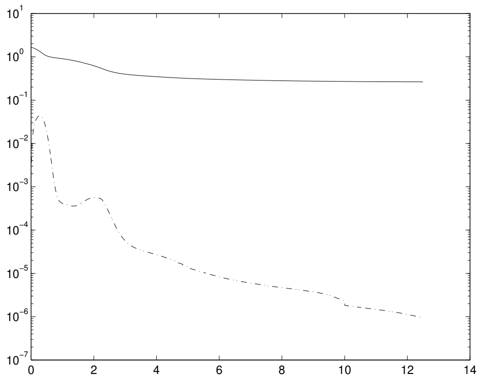

FIGURE 5.4. *Example 2. Decay of the residual (solid line) and kinetic energy;* $\Omega = (0,1)^2$, $\Delta x = 1/128$, $\Delta t = .001$, *and* $\delta = .01$.

Contour plots of the numerical solution u and the corresponding velocity v are shown in Figure 5.5. The order of magnitude of the velocity is about $|v|_\infty \approx 2\times 10^{-3}$.

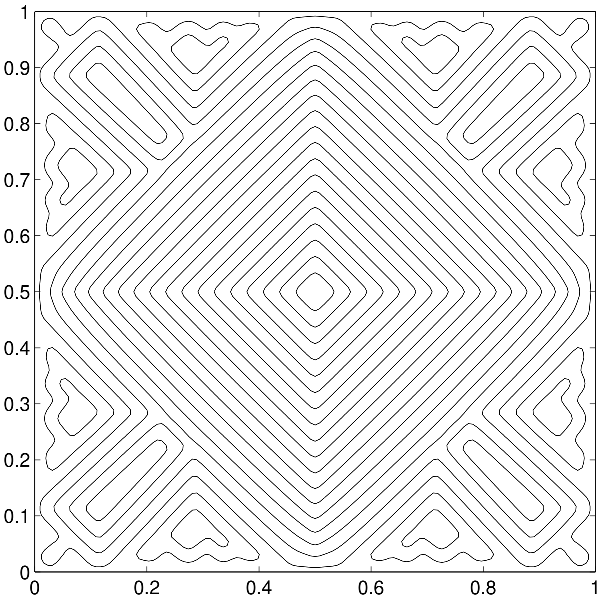

FIGURE 5.5A. *Example 2. Computed solution u;* $\Omega = (0,1)^2$, $\Delta x = 1/128$, $\Delta t = .001$, *and* $\delta = .01$.

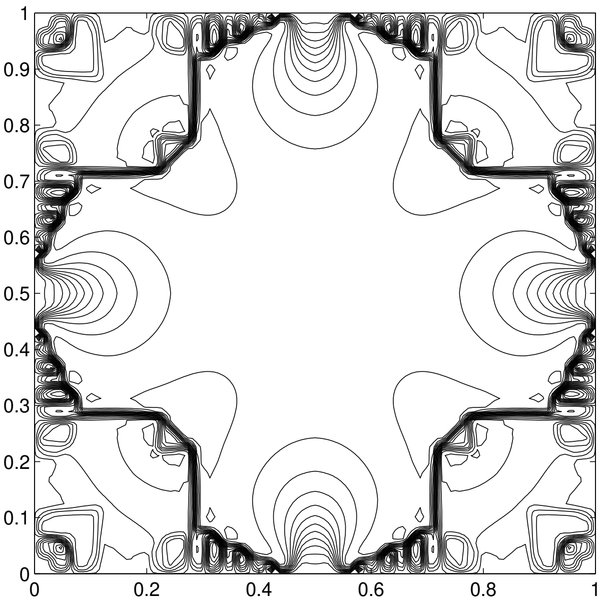

FIGURE 5.5B. *Example 2. Computed solution v;* $\Omega = (0,1)^2$, $\Delta x = 1/128$, $\Delta t = .001$, *and* $\delta = .01$.

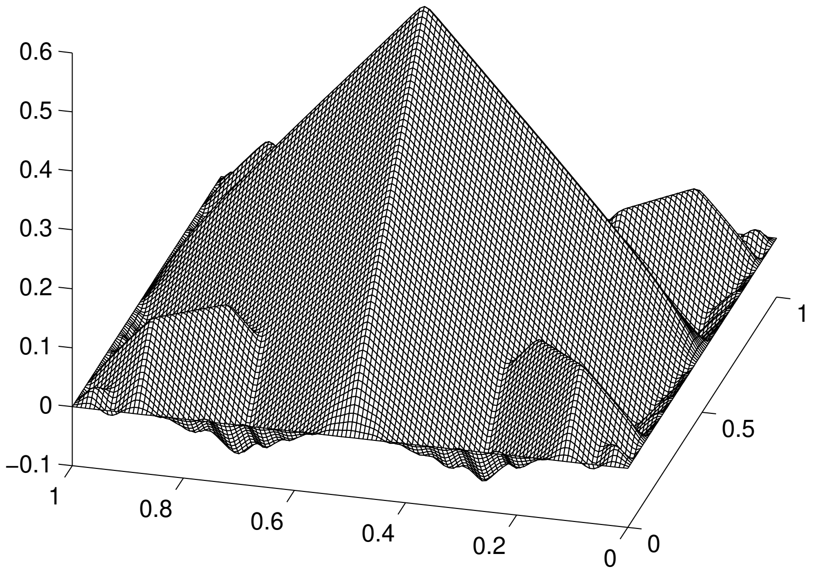

FIGURE 5.6. *Example 2. Computed solution $-u$; $\Omega = (0,1)^2$, $\Delta x = 1/128$, $\Delta t = .001$, and $\delta = .01$.*

For esthetic considerations, the numerical solution $-u$ was represented, instead of u, in Figure 5.6. The L^1-norm of the residual corresponding to the present experiment is about $\approx .264$.

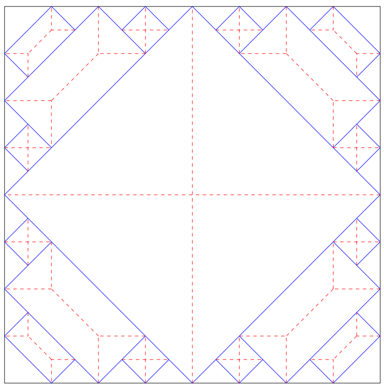

FIGURE 5.7. *Example 2. First three levels of refinement of an other solution.*

Some comments are in order. First, the solution obtained is neither (the approximation of) a viscosity solution, nor a "microstructure solution", i.e., a solution with oscillations at the level of the grid everywhere. It is in some sense in between. Second, since the problem consists, somehow, in tiling $\Omega = (0,1)^2$ with rectangles lined up with the main diagonals of Ω, one very natural guess might have been the structure displayed in Figure 5.7, which is obtained by, at each level, inserting the largest possible rectangles. The structure of the numerical solution is however clearly different, see Figure 5.6.

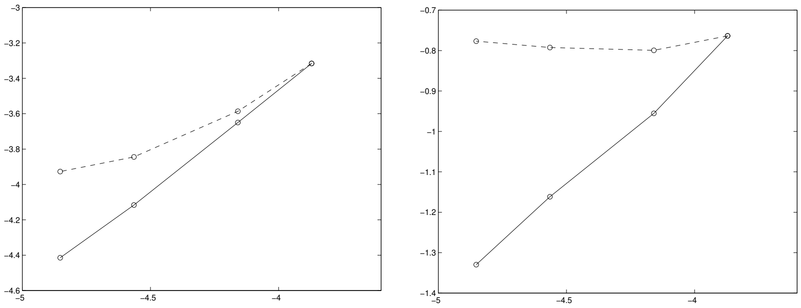

FIGURE 5.8. *Convergence rates upon refinement for Example 1 (left) and 2 (right),* $\log$*(residual) vs* $\log(\Delta x)$. δ *fixed: dashed curve;* $\delta = C\Delta x$*: solid curve.*

The convergence to steady state is much slower for Example 2 than it was for Example 1. This is partially explained by the fact that capillarity plays here a much more important role. This term penalizes jumps in the gradient of u, and thus limits the scale by preventing the total length of the lines of discontinuity of the gradient to grow without bound. In Example 1, our solution, which coincides with the viscosity solution, had clearly lines of discontinuity of finite length ($= 2\sqrt{(2)}$). For Example 2, the solution displayed in Figure 5.7 is such that this length blows up as more levels are considered. The numerical solution has an even more complicated behavior since, as can be seen from Figure 5.6, the tiles/rectangles are overlapping. The structure formation can be seen in the evolution of the kinetic energy displayed in Figure 5.4. The first burst, at about time $t \approx .3$ corresponds to the formation of the big pyramid. The same phenomenon was observed in Example 1. The next burst of kinetic energy, at about $t \approx 2$, appears during the formation of the next level of refinement.

The above remarks are further illustrated by a convergence study of our method for the two previous problems. Two types of calculations are presented. First, when the spatial mesh size Δx goes to zero, with a fixed capillarity coefficient δ, second, when Δx goes to zero with $\delta = C\Delta x$ (e.g. the same scaling as in [5]). The results are reported in Figure 5.8 in term of the L^1-norm of the residual. The stopping criterion was again "kinetic energy less than 10^{-6}". As expected for δ fixed, the main contribution to the energy, upon refinement of Δx, is eventually the capillarity term (last term in (3.11)). This explains why the corresponding curves in Figure 5.8 are levelling off. Finally, for $\delta = C\Delta x$, the method is clearly convergent, linearly for Example 1, sublinearly for Example 2, the difference reflecting again the nature of the curves of discontinuity of the gradient for both solutions.

Example 3: a vectorial nonconvex example. We solve the problem

$$\| \nabla u \|^2 = 2 \qquad \text{a.e. in } \Omega, \tag{5.3.1}$$

$$| \det \nabla u | = \Delta \qquad \text{a.e. in } \Omega, \tag{5.3.2}$$

$$u = 0 \qquad \text{on } \partial\Omega, \tag{5.3.3}$$

where $\Delta = 1/2$. As is easily checked, (5.3.1) and (5.3.2) are equivalent to

$$\mu_1(\nabla u) = \sqrt{1 - \sqrt{3}/2} \quad \mu_2(\nabla u) = \sqrt{1 + \sqrt{3}/2} \qquad \text{a.e. in } \Omega.$$

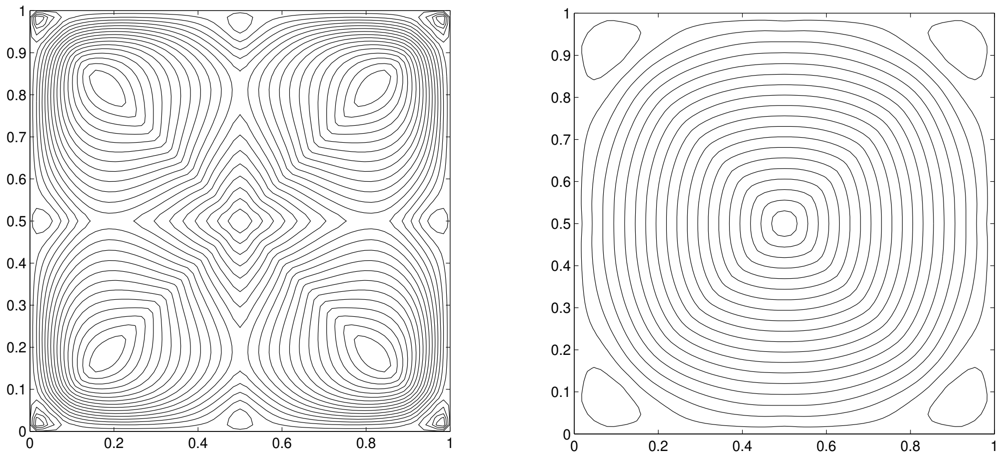

FIGURE 5.9. *Example 3. Computed solution u, first component on the left, second component on the right; $\Omega = (0,1)^2$, $\Delta x = 1/64$, $\Delta t = .001$, and $\delta = .01$.*

The domain Ω is again $(0,1)^2$ and the final discretization parameters were taken as $\Delta x = 1/64$, $\Delta t = .001$ and $\delta = .01$. Due to the complexity of the problem, several restarts, with increasingly small values of δ were necessary.

In the results presented below, the final (L^1 norms) of the residuals with respect to (5.3.1) and (5.3.2) were .0993 and .554. Contour plots of the two components of the numerical solution u are displayed in Figure 5.9, while the two components themselves (more precisely, $-u$) are shown in Figure 5.10.

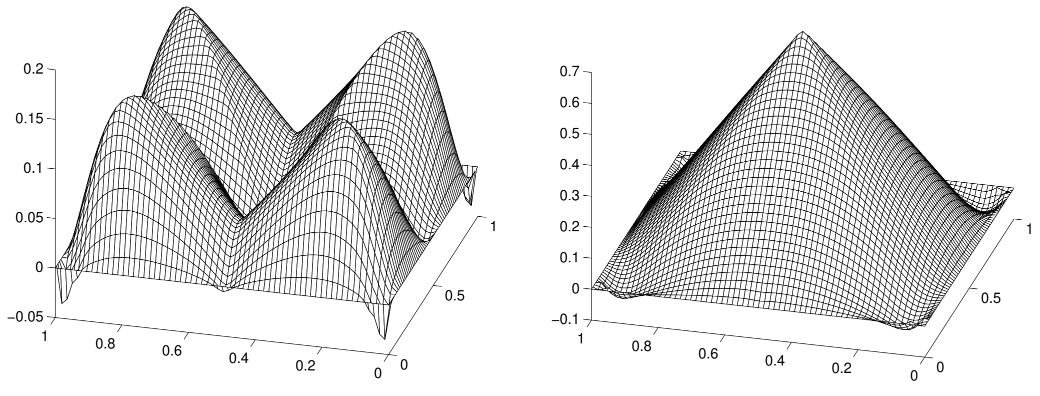

FIGURE 5.10. *Example 3. Computed solution $-u$, first component on the left, second component on the right; $\Omega = (0,1)^2$, $\Delta x = 1/64$, $\Delta t = .001$, and $\delta = .01$.*

The structure of the solution itself can be analyzed. The determinant $\det \nabla u$ is plotted in Figure 5.11.

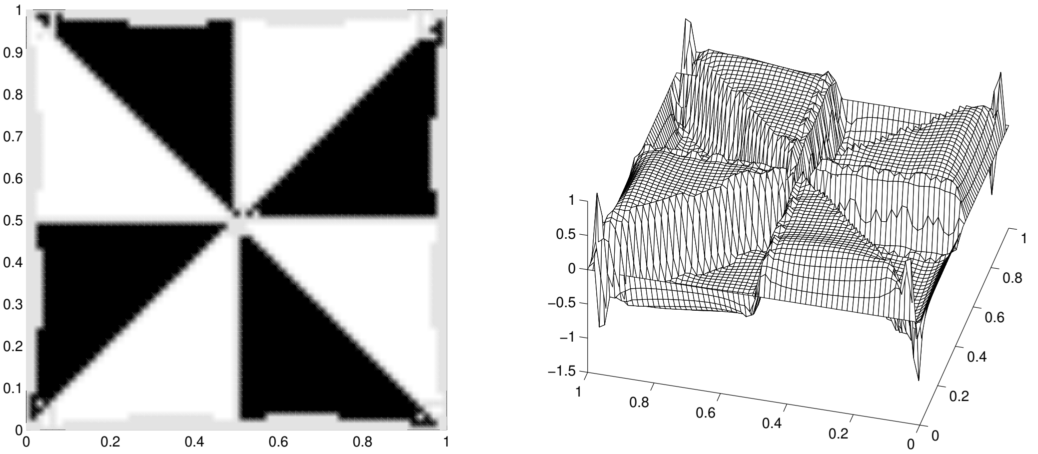

FIGURE 5.11. *Example 3. Values of the determinant* $\det \nabla u$*, black:* $\det \nabla u \approx 1/2$*, white:* $\det \nabla u \approx -1/2$*, grey: otherwise;* $\Omega = (0,1)^2$*,* $\Delta x = 1/64$*,* $\Delta t = .001$*, and* $\delta = .01$*.*

It is observed that proper ($\det \nabla u \approx \Delta = 1/2$) and improper ($\det \nabla u \approx -\Delta = -1/2$) matrices contribute equally to the construction of the solution. One can also measure the distance of the solution to the two "wells" defined by

$$F_0 = \begin{pmatrix} \sqrt{1-\sqrt{3}/2} & 0 \\ 0 & \pm\sqrt{1+\sqrt{3}/2} \end{pmatrix} \qquad F_1 = \begin{pmatrix} \sqrt{1+\sqrt{3}/2} & 0 \\ 0 & \pm\sqrt{1-\sqrt{3}/2} \end{pmatrix}.$$

More precisely, we measure, element by element, the quantity

$$\frac{\| \nabla u^T \nabla u - F_0^T F_0 \|^2}{\| \nabla u^T \nabla u - F_0^T F_0 \|^2 + \| \nabla u^T \nabla u - F_1^T F_1 \|^2}.$$

The results are displayed on Figure 5.12, and clearly indicates the "double well structure" of the solution.

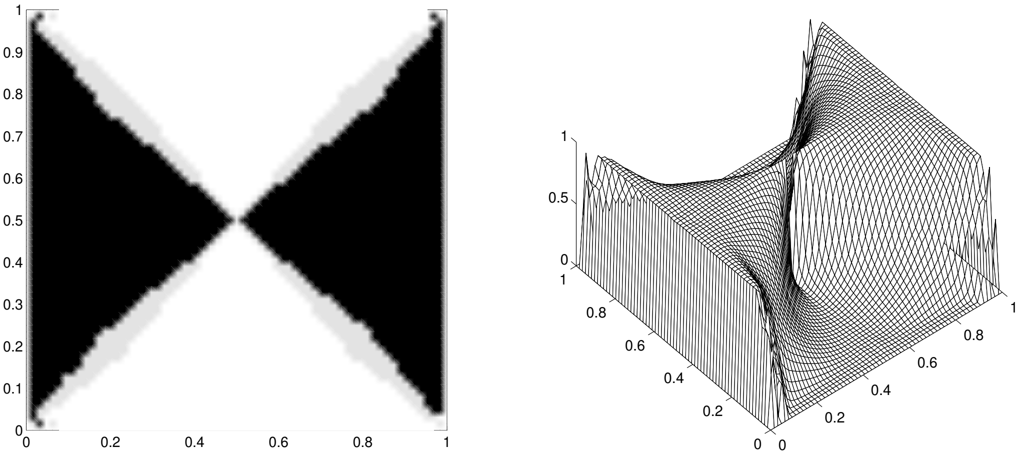

FIGURE 5.12. *Example 3. Double well structure of the solution black:* $\nabla u^T \nabla u$ *close to* $F_0^T F_0$*, white:* $\nabla u^T \nabla u$ *close to* $F_1^T F_1$*, grey: otherwise;* $\Omega = (0,1)^2$*,* $\Delta x = 1/64$*,* $\Delta t = .001$*, and* $\delta = .01$*.*

6. Conclusion. In this paper, we study how to construct numerical methods for scalar and vectorial Hamilton-Jacobi equations, when the viscosity approach is either ill-suited or not applicable. One of the main underlying question is: once a selection criterion is chosen, how can one make sure that the approximation process follows that criterion?

We work here with a viscoelasticity/capillarity criterion, common in Mechanics (see [5, 22, 28, 29, 31]). Three types of model problems are considered, namely, scalar convex, scalar nonconvex and vectorial nonconvex. The discretization is built on the principle according to which the low order terms in the truncation error should not perturbate the selection criterion. In other words, the numerical scheme must have a model equation whose solutions behave like those of the original problem [5]. That point was found to be essential through computational study, where low order methods were generally observed to significantly interfere with the nature of the solutions. Here, high order methods are not just "better", they seem to be necessary.

In [33], problems very close to our second model problem (scalar nonconvex) were considered. Our results differ sensibly from those for at least two reasons. First low order methods were used in [33], second, no capillarity effects were considered in [33]. As was recently proven in [29], viscoelasticity alone prevents the formation and/or motion of singularities. Both the results in [33] and ours are, not surprisingly, consistent with that.

Finally, we are not aware of other calculations for vectorial Hamilton-Jacobi equations of the type considered here. More work is needed to assess their use as alternate formulation for multiwell potential problems as those treated in [22].

Acknowledgments. This paper has greatly benefited from many discussions of various length and content with several people, among them Bernardo Cockburn, Bernard Dacorogna, Bob Kohn, Stan Osher, Piotr Rybka, Michael Shearer and Chi Wang Shu. Earlier calculations were performed on the Cray T90 of the North Carolina Supercomputing Center, whose support is gratefully acknowledged. Finally, the authors want to thank the referees for several remarks that led to a better presentation of those results.

REFERENCES

[1] J. M. Ball, *Dynamics and minimizing sequences*, in Problems involving change of type, Lecture Notes in Physics 359, K. Kirchgässner, ed., Springer, 1990, pp. 3–16.

[2] J. M. Ball and R. D. James, *Proposed experimental tests of a theory of fine microstructure and the two-well problem*, Phil. Trans. R. Soc. Lond. A, 338 (1992), pp. 389–450.

[3] R. E. Caflisch, Shi Jin, G. Russo, *Uniformly accurate schemes for hyperbolic systems with relaxation*, SIAM J. Numer. Anal., 34 (1997), pp. 246–281.

[4] A. Cellina and S. Perrotta, *On a problem of potential wells*, J. Conv. Anal., 2 (1995), pp. 103–115.

[5] B. Cockburn and Huuing Gau, *A model numerical scheme for the propagation of phase transitions in solids*, SIAM J. Sci. Comput., 17 (1996), pp. 1092–1121.

[6] M. G. Crandall, H. Ishii, and P. L. Lions, *User's guide to viscosity solutions of second order partial differential equations*, Bull. Amer. Math. Soc., 27 (1992), pp. 1–67.

[7] M. G. Crandall, and P. L. Lions, *Viscosity solutions of Hamilton-Jacobi Equations*, Trans. Amer. Math. Soc., 277 (1983), pp. 1–42.

[8] B. Dacorogna, and P. Marcellini, *Théorèmes d'existence dans les cas scalaire et vectoriel pour les équations de Hamilton-Jacobi*, C. R. Acad. Sci. Paris, Série 1, 322 (1996), pp. 237–240.

[9] B. Dacorogna, and P. Marcellini, *General existence theorems for Hamilton-Jacobi equa-*

tions in the scalar and vectorial cases, Preprint # 01.96, Département de Mathématiques, Ecole Polytechnique Fédérale de Lausanne, Switzerland. (1996).
[10] G. Friesecke and G. Dolzmann, *Implicit time discretization and global existence for a quasi-linear evolution equation with nonconvex energy*, SIAM J. Math. Anal., 28 (1997), pp. 363–380.
[11] G. Friesecke and J. B. McLeod, *Dynamics as a mechanism preventing the formation of finer and finer microstructure*, Arch. Rational Mech. Anal., 133 (1996), pp. 199–247.
[12] E. Hairer, S. P. Nørsett and G. Wanner, *Solving ordinary differential equations I*, Springer Verlag, 1987.
[13] E. Hairer, G. Wanner, *Solving ordinary differential equations II*, Springer Verlag, 1991.
[14] B. T. Hayes and P. G. LeFloch, *Non-classical shock waves in scalar conservation laws*, Arch. Rat. Mech. Anal., to appear.
[15] C. Hirsch, *Numerical computation of internal and external flows, Volume 1*, Wiley, 1988.
[16] A. Iserles, *Stability and dynamics of numerical methods for nonlinear ordinary differential equations*, IMA J. Numer. Anal., 10 (1990), pp. 1–30.
[17] C. T. Kelley, *Iterative methods for linear and nonlinear equations*, Frontiers in Applied Mathematics, #16, SIAM, 1995.
[18] P. Klouček and M. Luskin, *The computation of the dynamics of martensitic microstructure*, Continuum Mech. Thermodyn., 6 (1994), pp. 209–240.
[19] R.V. Kohn and Weimin Jin, *Private communication.*
[20] S. N. Kruskov, *Generalized solutions of the Hamilton-Jacobi equations of Eikonal type. 1. Formulation of the problems; existence, uniqueness and stability theorems; some properties of the solutions*, Math. USSR Sbornik, 27 (1975), pp. 406–446.
[21] P. L. Lions, *Generalized solutions of Hamilton-Jacobi equations*, Research Notes in Mathematics, #69, Pitman, Boston, 1982.
[22] M. Luskin, *On the computation of crystalline microstructure*, Acta Numerica, 5 (1996), pp. 191–257.
[23] K. W. Morton, *Stability of finite difference approximations to a diffusion-convection equation*, Int. J. Numer. Meth. Eng., 15 (1980), pp. 677–683.
[24] R. A. Nicolaides, N. Walkington and Han Wang, *Numerical methods for a nonconvex optimization problem modeling martensitic microstructure*, SIAM J. Sci. Comput., 18 (1997), pp. 1122–1141.
[25] M. Ortiz and G. Gioia, *The morphology and folding patterns of buckling-driven thin-film blisters*, J. Mech. Phys. Solids, 42 (1994), pp. 531–559.
[26] S. Osher and J. A. Sethian, *Fronts propagating with curvature-dependent speed: algorithms based on Hamilton-Jacobi formulations*, J. Comput. Phys., 79 (1988), pp. 12–49.
[27] S. Osher and Chi-Wang Shu, *High-order essentially nonoscillatory schemes for Hamilton-Jacobi equations*, SIAM J. Numer. Anal., 28 (1991), pp. 907–922.
[28] P. Rybka, *Dynamical modelling of phase transitions by means of viscoelasticity in many dimensions*, Proc. R. Soc. Edinburgh, 121A (1992), pp. 101–138.
[29] P. Rybka, *The viscous damping prevents propagation of singularities in the system of viscoelasticity*, Proc. R. Soc. Edinburgh, 127A (1997), to appear.
[30] P. Rybka, *Private communication.*
[31] P. Rybka and K. H. Hoffmann, *Asymptotics for an equation related to martensitic phase transitions*, Preprint TUM-M9706, Technische Universität München (1997).
[32] J. Stoer and R. Bulirsch, *Introduction to Numerical Analysis, Second Edition*, Texts in Applied Mathematics, #12, Springer Verlag, 1993.
[33] P. J. Swart and P. J. Holmes, *Energy minimization and the formation of microstructure in dynamic anti-plane shear*, Arch. Rational Mech. Anal, 121 (1992), pp. 37–85.
[34] H. C. Yee and P. K. Sweby, *Global asymptotic behavior of iterative implicit schemes*, International J. of Bifurcation and Chaos, 4 (1994), pp. 1579–1611.
[35] H. C. Yee and P. K. Sweby, *Dynamical approach study of spurious steady-state numerical solutions of nonlinear differential equations II. Global asymptotic behavior of time discretizations*, Comp. Fluid Dyn., 4 (1995), pp. 219–283.